

VIP Urea Electrosynthesis Very Important Paper

How to cite: *Angew. Chem. Int. Ed.* **2021**, *60*, 10910–10918

International Edition: doi.org/10.1002/anie.202101275

German Edition: doi.org/10.1002/ange.202101275

Unveiling Electrochemical Urea Synthesis by Co-Activation of CO₂ and N₂ with Mott–Schottky Heterostructure Catalysts

Menglei Yuan⁺, Junwu Chen⁺, Yiling Bai, Zhanjun Liu, Jingxian Zhang, Tongkun Zhao, Qin Wang, Shuwei Li, Hongyan He, and Guangjin Zhang*

Abstract: Electrocatalytic C–N bond coupling to convert CO₂ and N₂ molecules into urea under ambient conditions is a promising alternative to harsh industrial processes. However, the adsorption and activation of inert gas molecules and then the driving of the C–N coupling reaction is energetically challenging. Herein, novel Mott–Schottky Bi–BiVO₄ heterostructures are described that realize a remarkable urea yield rate of 5.91 mmol h⁻¹ g⁻¹ and a Faradaic efficiency of 12.55 % at -0.4 V vs. RHE. Comprehensive analysis confirms the emerging space-charge region in the heterostructure interface not only facilitates the targeted adsorption and activation of CO₂ and N₂ molecules on the generated local nucleophilic and electrophilic regions, but also effectively suppresses CO poisoning and the formation of endothermic *NNH intermediates. This guarantees the desired exothermic coupling of *N=N* intermediates and generated CO to form the urea precursor, *NCON*.

Introduction

Nitrogen is regarded as an indispensable element for all life, which accounts for 78 % of the atmosphere but can't be directly adopted by plants and animals.^[1] Transforming N₂ into valuable fertilizer under mild conditions is highly anticipated for human beings.^[2] On the other hand, excessive carbon dioxide (CO₂) emissions have aroused severe environmental concerns.^[3] Therefore, converting both N₂ and CO₂ into value-added urea molecules via C–N coupling reaction under ambient conditions is a promising route to achieve both carbon balance strategy and high-value utilization of CO₂.^[4] Nonetheless, the chemical inert of N₂ (N≡N, 940.95 kJ mol⁻¹) and CO₂ (C=O, 806 kJ mol⁻¹) inevitably impede the activation

of N₂/CO₂ molecules.^[5] To this end, tremendous efforts have been devoted to converting N₂ and CO₂ to value-added chemical products and fuels (NH₃, N₂H₂, CH₃OH, CH₃COOH, etc.).^[6] Compared with the conventional thermal catalytic and other hydrogenation processes, the utilization of the electrochemical approach exhibits great advantages in atom and energy economies.^[7] It thus motivates researchers to construct an electrochemical C–N bond coupling system by directly using CO₂ and amine derivatives/nitrogen sources (nitrate, nitrite, NO, and even N₂) as feedstock.^[8]

When feeding with N₂ and CO₂ as the reactant, the electrochemical C–N coupling reactions can proceed to produce valuable urea [CO(NH₂)₂] molecules, which is regarded as one of the most efficient nitrogen fertilizer and is of great significance to the chemical industry.^[9] The industrial urea synthesis is dominated by two consecutive steps, including N₂ + H₂ → NH₃ and followed by NH₃ + CO₂ → CO(NH₂)₂, which operated at harsh reaction conditions (350–550 °C, 150–350 bar and 150–200 °C, 150–250 bar, respectively).^[10] Compared with huge energy consumption industrial processes, the electrochemical urea synthesis provides an appealing route (N₂ + CO₂ + 6H⁺ + 6e⁻ → CO(NH₂)₂ + H₂O) under mild conditions.^[4] However, the related catalytic activity and selectivity for electrochemical urea synthesis are still extremely low. The main challenges can be ascribed as i) extraordinarily weak chemical adsorption of inert CO₂/N₂ on the catalysts surface;^[11] ii) the dissociation of highly stable C=O bond and N≡N bond requires high overpotential;^[5c,12] iii) the parallel CO₂/N₂ reduction reactions strongly competes with the desired C–N coupling reaction for urea synthesis and further results in the complex product distribution.^[7]

[*] M. Yuan,^[†] J. Chen,^[†] J. Zhang, T. Zhao, S. Li, Prof. H. He, Prof. G. Zhang
 CAS Key Laboratory of Green Process Engineering
 State Key Laboratory of Multiphase Complex Systems
 Institute of Process Engineering, Chinese Academy of Sciences
 Beijing 100190 (P. R. China)
 E-mail: zhanggj@ipe.ac.cn

M. Yuan,^[†] J. Chen,^[†] Prof. Z. Liu, J. Zhang, T. Zhao, S. Li, Prof. H. He, Prof. G. Zhang
 Center of Materials Science and Optoelectronics Engineering
 University of Chinese Academy of Sciences
 Beijing 100049 (P. R. China)

Y. Bai, Prof. Z. Liu
 CAS Key Laboratory of Carbon Materials
 Institute of Coal Chemistry, Chinese Academy of Sciences
 Taiyuan 030001 (P. R. China)

Y. Bai
 SynCat@Beijing, Synfuels China Technology Co. Ltd
 Beijing 101407 (P. R. China)

Q. Wang
 Engineering Design Department, Hebei Enco Petrochemical Engineering Co. Ltd., Henan Branch
 Henan 450000 (P. R. China)

Prof. G. Zhang
 Chemistry and Chemical Engineering Guangdong Laboratory
 Shantou 515031 (P. R. China)

[*] These authors contributed equally to this work.

 Supporting information and the ORCID identification number(s) of the author(s) of this article can be found under:
 <https://doi.org/10.1002/anie.202101275>.

Aiming at this challenging field, Chen et al. reached the urea production rate of $3.36 \text{ mmol g}^{-1} \text{ h}^{-1}$ and Faradaic efficiency (FE) of 8.92% at -0.4 V vs. RHE on PdCu/TiO₂ hybrids.^[4] Despite the aforementioned noble metal Pd-based catalysts that can realize urea electrosynthesis, the related electrocatalytic activity still needs to be improved. Besides, their real application in large-scale is restricted by high cost and scarcity. Therefore, it is highly anticipated to develop earth-abundant alternatives to further improve urea electrosynthesis performance. The electrochemical C-N coupling reaction in urea synthesis is strongly dependent on the surface electronic state of electrocatalysts. Designing the electrocatalyst to enhance the adsorption and activation of inert gas molecules can be adopted as a promising strategy to promote C-N coupling reaction and further urea formation.^[13] Thus, we supposed that Mott–Schottky heterostructures may provide a new possibility to enhance the electrocatalytic capability of urea synthesis.^[14] The reason can be ascribed to the formed interface can stimulate spontaneous charge transfer and then generate a special space-charge region to drive the targeted surface reaction. The band bending at the interface facilitates the charge redistribution until the electrocatalytic system reaches a thermal equilibrium state. Then, the oppositely charged regions arise at the heterointerface and bring about the alteration of electron density around the interface, which is favorable for the adsorption of targeted small molecules (CO₂/N₂) and the subsequent protonation process.^[15] Accordingly, engineering distinct space-charge regions in Mott–Schottky heterojunction would be the feasible strategy for remarkable urea electrosynthesis but it hasn't been investigated so far.

Herein, as the proof-of-concept catalyst, Mott–Schottky heterostructural Bi-BiVO₄ hybrids were prepared by the NaBH₄ reduction strategy and ensured spontaneous electron transfer from BiVO₄ to Bi. The rationally engineering space-charge region guarantees the accurate adsorption and activation of N₂ and CO₂ and further promotes the desired electrochemical C-N coupling reaction in urea synthesis. Therefore, the as-prepared Mott–Schottky Bi-BiVO₄ heterostructure electrocatalysts deliver a remarkable urea production rate of $5.91 \text{ mmol h}^{-1} \text{ g}^{-1}$ with a FE of 12.55% at -0.4 V (vs. RHE), outperforming those reported best values. This work underlines the significance of the engineering space-charge region for enhancing urea synthesis by electrocatalytic C-N coupling reaction.

Results and Discussion

The pristine BiVO₄ was directly prepared by reacting bismuth nitrate with ammonium metavanadate by in situ redox route. Figure 1a displays the X-ray diffraction (XRD) patterns of as-prepared pristine BiVO₄ match well with monoclinic phase of BiVO₄ (JCPDS: 83-1700). The corresponding crystal structure contains BiO₁₀ decahedron and VO₄ tetrahedron units (Figure S1). When the pristine BiVO₄ is partially reduced by the NaBH₄, the Bi-BiVO₄ hybrids were obtained which only exhibit relatively weak BiVO₄ diffraction peaks compared to pristine BiVO₄ (Figure 1b). The reason

can be attributed to the reduction by NaBH₄ that inducing abundant defect BiO₁₀ decahedron models until the formation of metallic Bi site. As displayed in the Raman spectrum (Figure 1c), the pronounced peaks detected at 327 and 367 cm⁻¹ correspond to asymmetric and symmetric stretching modes of VO₄³⁻ tetrahedron unit in BiVO₄. Besides, the short (B_g) and long (A_g) asymmetric V-O stretching modes also appear at 637 and 702 cm⁻¹.^[16] The intense Raman peak that emerged at 826 cm⁻¹ can be ascribed to the shorter symmetric V-O stretching mode (A_g).^[17] Compared with pristine BiVO₄, the disappearance of the vibration peaks in Bi-BiVO₄ hybrids at 367, 637, and 702 cm⁻¹ results from damages to the inherent crystal structure of BiVO₄ by the reaction of NaBH₄. Although the BiO₁₀ decahedron units were undermined and thus produced Bi site, the XRD diffraction peaks of metallic Bi can't be found in Bi-BiVO₄ hybrids, which can be ascribed to the high dispersion and low concentration of metallic Bi. To further certify the existence of metallic Bi, X-ray photoelectron spectroscopy (XPS) of the hybrids was examined. It is shown that the metallic Bi⁰ peak can be detected at 162.1 eV for Bi-BiVO₄ hybrids in the Bi 4f region.^[18] Besides, the characteristic peaks located at 159.3 eV and 164.7 eV can be assigned to Bi³⁺ 4f_{7/2} and Bi³⁺ 4f_{5/2}, respectively (Figure 1d).^[18b] The V 2p spectrum can be deconvoluted into V⁴⁺ 2p (515.8 eV) peak (Figure 1e).^[19] Notably, the Bi³⁺ 4f and V⁴⁺ 2p peaks in Bi-BiVO₄ hybrids show the negative shift of 0.2 eV and positive shift of 0.2 eV respectively, compared with pristine BiVO₄, originating from the electronic interaction between metallic Bi⁰ phase and BiVO₄. Mott–Schottky test was further utilized to reveal the electron transfer in Bi-BiVO₄ hybrids (Figure 1f). BiVO₄ samples possess a positive slope, reflecting typical n-type semiconductor characteristics. Thus, when it was combined with metallic Bi, the unique Mott–Schottky heterostructure can be formed and the electrons can transfer from BiVO₄ to metallic Bi to form a unique space-charge region (Figure 1g and Figure S2a–c). The fabricated space-charge region ensures the effective synthesis of urea at different active sites. Additionally, the NaBH₄ reduction strategy also results in the increase of Brunauer-Emmett-Teller (BET) specific surface area from $14.7 \text{ m}^2 \text{ g}^{-1}$ (BiVO₄) to $30.4 \text{ m}^2 \text{ g}^{-1}$ (Bi-BiVO₄) (Figure 1h).

The field-emission scanning electron microscopy (FE-SEM) image in Figure 2a reveals that pristine BiVO₄ possesses an average width and length of 400 nm and 1 μm, respectively. The corresponding EDS mapping confirms the uniform distribution of Bi, V, and O elements (Figure 2b), which is consistent with the XPS survey spectrum (Figure 1i). The lattice spacing (0.312 nm) in high-magnification transmission electron microscopy (HRTEM) corresponds to the (130) crystal plane of BiVO₄ (Figure S2d). Figure 2d,e proves that the Bi-BiVO₄ hybrids still maintain a similar morphology and uniform element distribution with pure BiVO₄, but the unique heterostructural interfaces between metallic Bi and BiVO₄ can be observed (Figure 2c and f). The formation of such heterojunction creates the unique space-charge region (Figure S2c) with self-driven charge transfer from BiVO₄ to Bi. Thus local electrophilic and nucleophilic regions are generated.

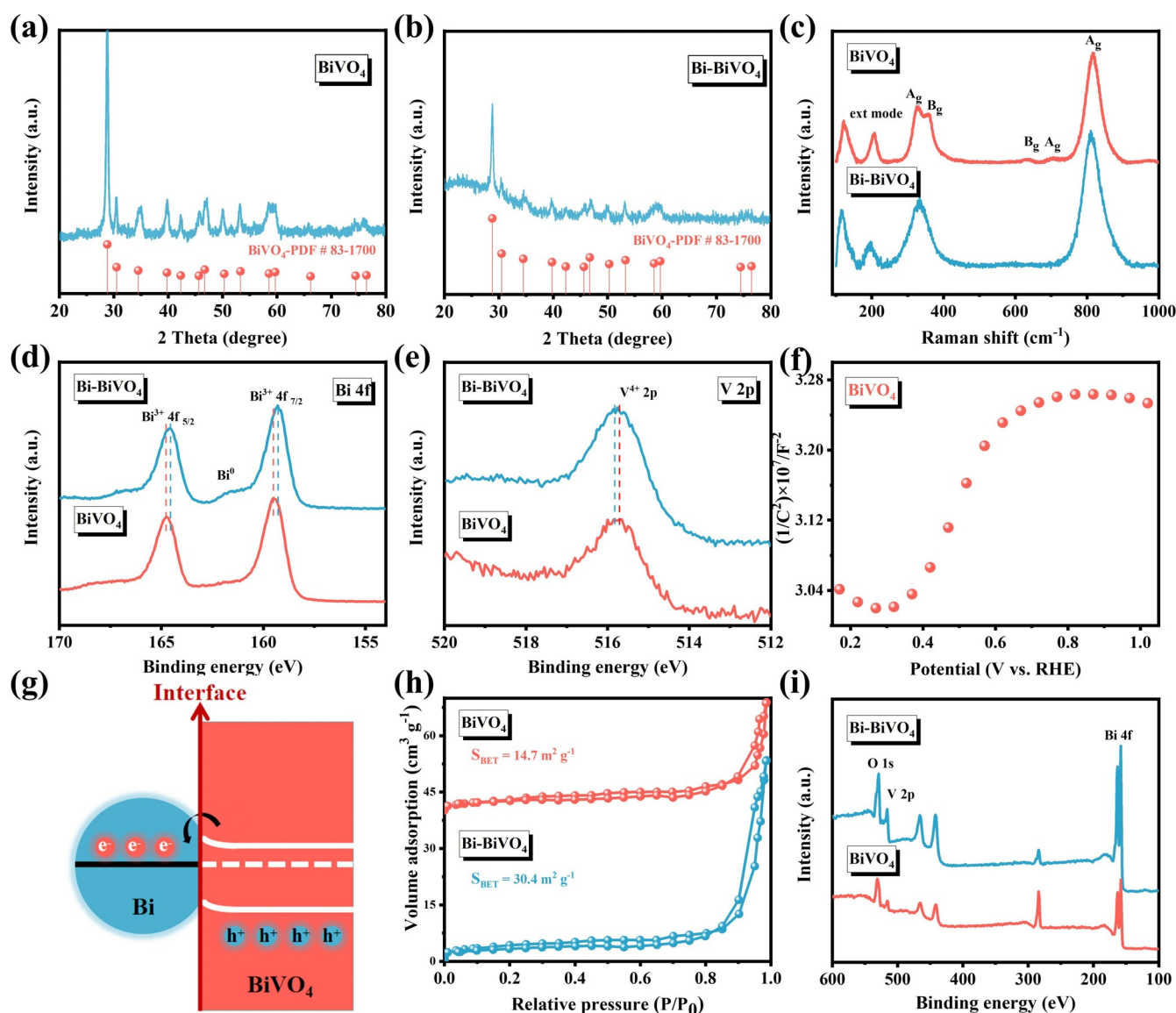


Figure 1. XRD patterns of a) BiVO_4 and b) Bi-BiVO_4 ; c) Raman spectra, d) high-resolution Bi 4f spectra and e) high-resolution V 2p spectra of BiVO_4 and Bi-BiVO_4 ; f) Mott–Schottky plots of BiVO_4 ; g) schematic illustration of the charge transfer process in Bi-BiVO_4 ; h) BET specific surface area and i) XPS survey spectra of BiVO_4 and Bi-BiVO_4 .

As for electrocatalytic urea synthesis, N_2 and CO_2 as feeding gas were continuously bubbled into the H-shaped cell, which is separated by the Nafion 211 membrane and equipped with a three-electrode system (Figure S3). Linear sweep voltammetry (LSV) was used to preliminarily evaluate the potential performance of urea electrosynthesis with Bi-BiVO_4 hybrids. As displayed in Figure 3a, the Bi-BiVO_4 hybrids exhibit an enhanced current density in mixed gas ($\text{N}_2 + \text{CO}_2$)-saturated 0.1 M KHCO_3 solution relative to sole gas (N_2/CO_2)-saturated electrolyte, indicating the occurrence of electrocatalytic urea synthesis. It has been reported that the electrochemical urea production ability of the catalyst was dominated by effectively coupling carbon dioxide reduction reaction (CO_2RR) with nitrogen reduction reaction (NRR).^[4] In another word, encouraging electrocatalytic NRR and CO_2RR performance of the Bi-BiVO_4 hybrids guarantee the

electrocatalytic production of urea process (Figure 3b,c). Constant potential electrolysis ranging from -0.3 V to -0.7 V vs. RHE were selected to further quantitatively assess urea electrosynthesis activity. The time-dependent current density curves recorded for 2 h at various potentials illustrate the superior stability of Bi-BiVO_4 hybrids (Figure S4). The generated urea and by-product NH_3 were estimated by the diacetyl monoxime method and indophenol blue method, the related calibration curves are depicted in Figure S5.^[20] Besides, the possible gas products such as H_2 and CO were monitored by on-line gas chromatography. The calculated urea yield rate and Faradaic efficiency (FE) in Figure 3d demonstrate that when the potential reached -0.4 V vs. RHE, the Bi-BiVO_4 hybrids electrode delivers the maximum urea yield rate of $5.91 \text{ mmol h}^{-1} \text{ g}^{-1}$ and FE of 12.55%. As listed in Table S1, the electrocatalytic urea synthesis perfor-

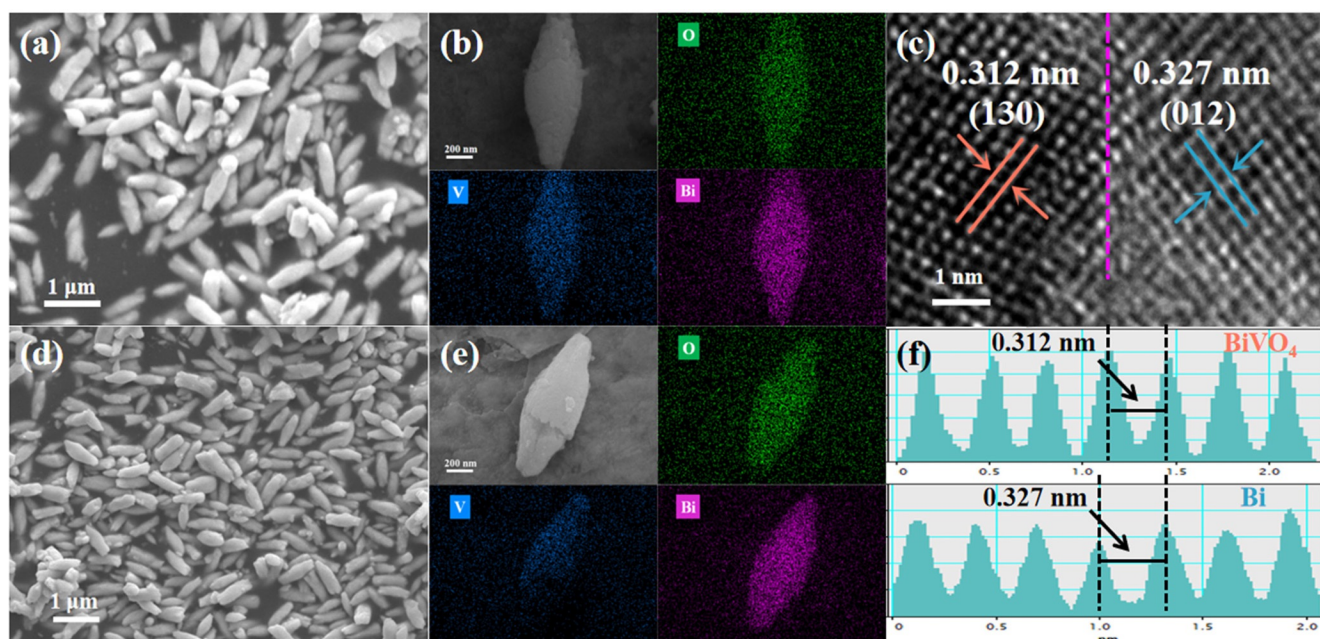


Figure 2. a) SEM image and b) the corresponding element mapping of BiVO_4 ; c) high-magnification TEM image of Bi-BiVO_4 hybrids and the dotted line represents the heterointerfaces; d) SEM image and e) the corresponding element mapping of Bi-BiVO_4 hybrids; f) the well-resolved lattice fringe of Bi-BiVO_4 hybrids in (c).

mance of Bi-BiVO_4 hybrids is superior to the highest values reported so far. However, as the potential shifted below -0.4 V, the excessive release of CO occupied the adsorption sites for CO_2 and N_2 result in dramatically reduced urea yield and FE and further bring about the diversified reduction products distribution (Figure 3e). Note that Bi-BiVO_4 hybrids deliver the highest FE (15.33%) and NH_3 yield rate ($7.07 \text{ mmol h}^{-1} \text{ g}^{-1}$) at -0.4 V vs. RHE during NRR, which are higher than that of the electrocatalytic urea synthesis process (Figure 3b). The reason can be attributed to the modulated reaction pathways to promote electrochemical C-N coupling reaction and further generate urea, which will be further revealed by DFT calculations. Furthermore, a 10 h chronoamperometry test (Figure S6) and cycling experiments (Figure S7) were utilized to evaluate the durability of Bi-BiVO_4 hybrids. Negligible degradation in current density and electrocatalytic activity indicates the desirable stability of Bi-BiVO_4 hybrids. The related characterizations also prove that the obtained Bi-BiVO_4 hybrids still maintain their original morphology, chemical state, and crystal phase after 10 h continuous electrolysis (Figure S8). Besides, benefiting from the enhanced solubility of CO_2 in ionic liquid (IL, 1-butyl-3-methylimidazolium tetrafluoroborate),^[21] the IL- KHCO_3 was used as the electrolyte and the system exhibited the urea yield rate of $6.64 \text{ mmol h}^{-1} \text{ g}^{-1}$ and FE of 15.8% at -0.4 V vs. RHE, which are higher than that in pure KHCO_3 solution (Figure S9a).

Since adventitious NO_x is inevitably present in the environment and chemicals which may lead to false-positive results, a series of control experiments were conducted to further verify the generated urea comes from the simultaneous reduction of CO_2 and N_2 rather than contaminants (Scheme 1 and Figure S9b). Additionally, the capability of Bi-

BiVO_4 hybrids to synergistically activate CO_2 and N_2 molecules was further proved by isotope labeling experiments. No distinguished $\text{CO}(\text{NH}_2)_2$ signal was observed when utilizing $^{15}\text{N}_2$ and CO_2 as the feeding gas, only $\text{CO}(^{15}\text{NH}_2)_2$ signal was detected in the reacted electrolyte, confirming that urea was generated by simultaneous reduction of CO_2 and N_2 (Figure 3f). Besides, the concentration of $\text{CO}(^{15}\text{NH}_2)_2$ after 2 h electrolysis was also quantitatively detected based on the peak area of ^1H NMR (Figure 3g,h). As expected, the calculated $\text{CO}(^{15}\text{NH}_2)_2$ concentration is in good accordance with that detected by the diacetyl monoxime method (Figure 3i). All these results convincingly confirm the reduction of both N_2 and CO_2 into urea was catalyzed by Bi-BiVO_4 hybrids.

To uncover the contribution of engineering space-charge region on the enhancement of Bi-BiVO_4 hybrids performance, the electrochemical properties of pristine BiVO_4 were also investigated. As expected, it can be seen in Figure 4a that pristine BiVO_4 displays remarkably decreased urea yield and FE in comparison with Bi-BiVO_4 hybrids. In Figure 4b and Figure S10, the Bi-BiVO_4 hybrids also exhibit a larger electrochemical active surface area (ECSA) than that of pristine BiVO_4 , illustrating that the designed space-charge region is favorable for the exposure of more active sites.^[22] Furthermore, the electrochemical impedance spectroscopy (EIS) of the Bi-BiVO_4 hybrids delivers smaller semicircle and higher slope compared with that of pristine BiVO_4 , which verify that Bi-BiVO_4 hybrids coupled with space-charge region facilitate the effective charge transfer and thus endow the Bi and BiVO_4 surface with a local nucleophilic and electrophilic region (Figure 4c).^[23] As the chemisorption of N_2 and CO_2 are regarded as the initial step towards urea electrosynthesis, it is critical to promote the chemisorption ability of N_2 and CO_2 on

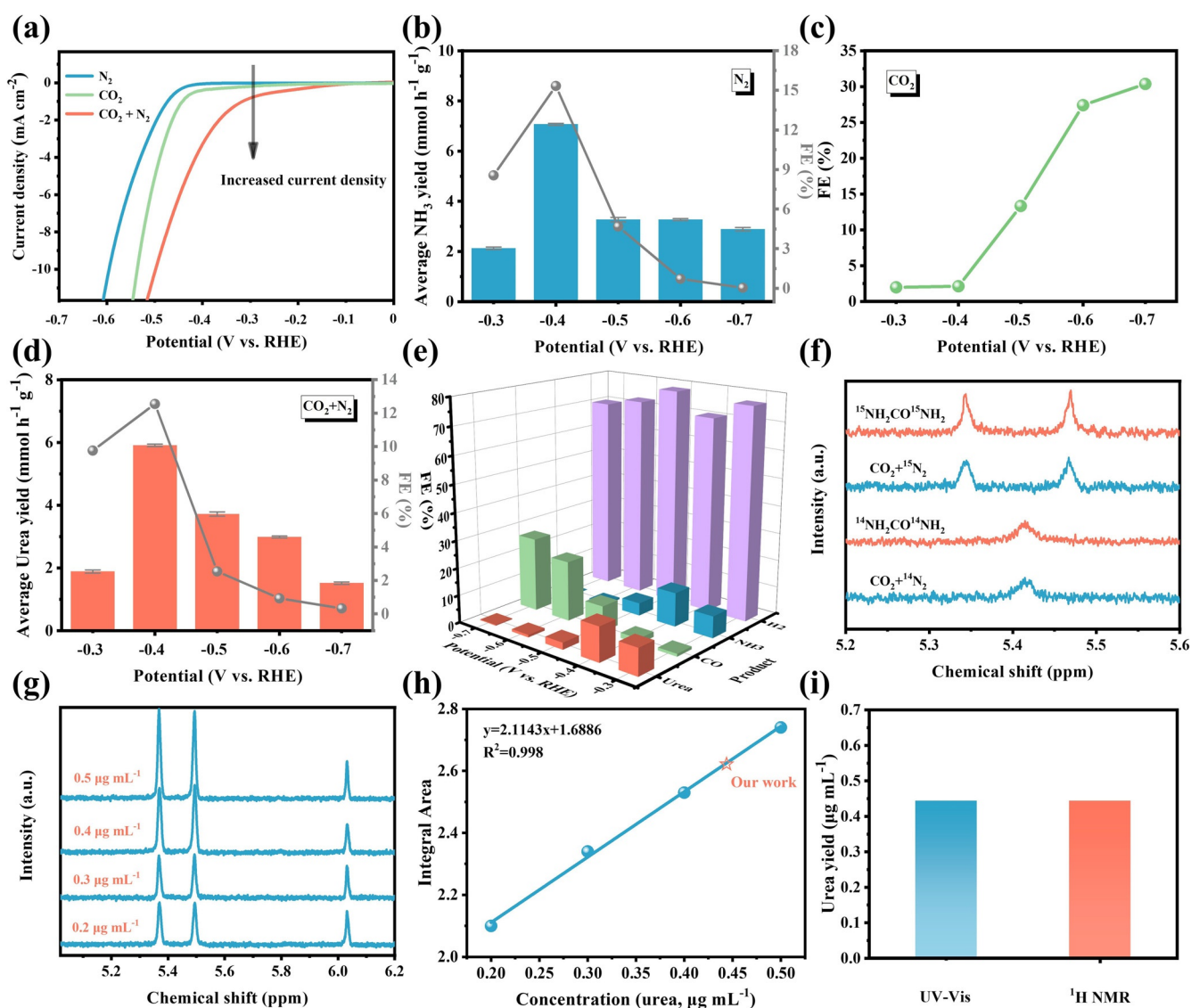


Figure 3. a) LSV curves of Bi-BiVO₄ hybrids at N₂, CO₂, and N₂ + CO₂ saturated electrolyte; b) NH₃ synthesis with N₂ as the feeding gas and c) CO generation with CO₂ as the feeding gas at various potentials for Bi-BiVO₄ hybrids; d) the urea yield rate and Faradic efficiencies and e) the corresponding product distribution of H₂ (purple), CO (cyan-blue), NH₃ (blue), and urea (red) with N₂ and CO₂ as the feeding gas at various potentials for Bi-BiVO₄ hybrids; f) ¹H NMR spectra of electrolyte saturated with ¹⁵N₂ + CO₂ / ¹⁴N₂ + CO₂ after 2 h electrolysis and standard ¹⁵NH₂CO¹⁵NH₂ / ¹⁴NH₂CO¹⁴NH₂ solution; g) ¹H NMR spectra of standard ¹⁵NH₂CO¹⁵NH₂ solution with various concentrations of 0.2–0.5 μg mL⁻¹; h) integral area (¹⁵NH₂CO¹⁵NH₂/C₄H₄O₄) concentration linear relation calibrated using standard ¹⁵NH₂CO¹⁵NH₂ solution; i) the urea yield of Bi-BiVO₄ hybrids after 2 h electrolysis detected by UV/Vis and ¹H NMR spectroscopy.

the electrocatalysts. In this work, engineering space-charge regions would be served as a promising strategy toward significantly enhancing the chemisorption capability of inert N₂ and CO₂ molecules. As revealed by theoretical simulations, the electron-rich N atom in N₂ and electron-deficient C atom in CO₂ (Figure 4d) will target adsorb on the generated electrophilic and nucleophilic regions in Bi-BiVO₄ hybrids due to electronic interaction.^[24] As shown in Figure 4 e,f, both the N₂- and CO₂-TPD spectrum of Bi-BiVO₄ hybrids display the stronger binding strength and larger adsorption peak as compared to that of pristine BiVO₄, verifying the enhancement of the adsorption capacity for both N₂ and CO₂ molecules on Bi-BiVO₄ hybrids.^[25]

The density functional theory (DFT) calculations were further carried out to corroborate the contribution of the space-charge region to adsorb and activate inert gas molecules. To this end, the adsorption behavior of reactant molecules on the two different optimized structures was firstly investigated. As revealed by Bader charge analysis (Figure 5 a), the presence of space-charge region in Bi-BiVO₄ hybrids guarantees the spontaneous electron transfer from BiVO₄ to Bi (1.21 e⁻), in agreement with the above XPS and Raman characterizations. The corresponding charge accumulation and depletion endows the Bi and BiVO₄ interface with the local nucleophilic and electrophilic region, which achieves the targeted adsorption of gas molecules by the electrostatic interaction. As expected, the adsorption energies of both N₂

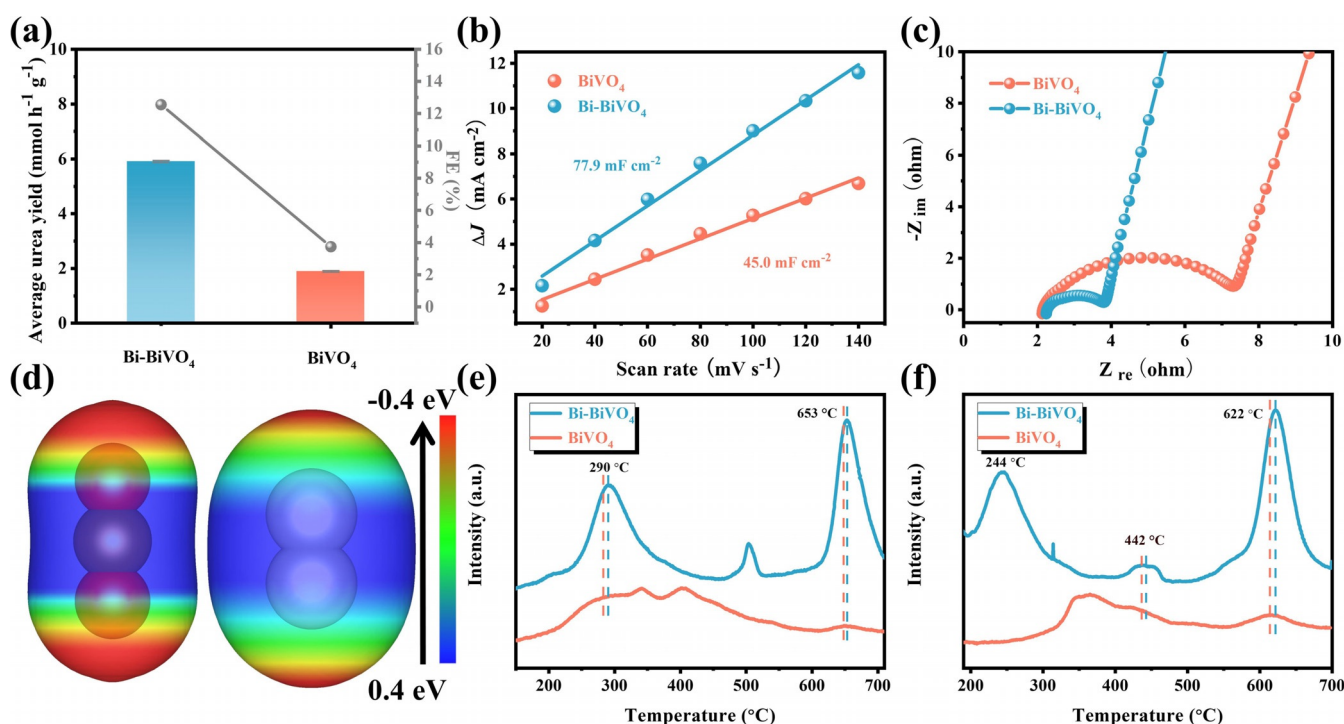


Figure 4. a) Average urea yield rate and FE; b) ΔJ of electrocatalysts plotted against scan rate at -0.05 V vs. RHE; c) Nyquist plots of electrochemical impedance spectra (EIS) of BiVO₄ and Bi-BiVO₄; d) electron density isosurface of CO₂ molecule (left) and N₂ molecule (right), the color bar represents the electrostatic potential scale; e) nitrogen temperature-programmed desorption (N₂-TPD) plots and f) carbon dioxide temperature-programmed desorption (CO₂-TPD) plots for BiVO₄ and Bi-BiVO₄.

and CO₂ on the pristine BiVO₄ model are much higher than that of Bi-BiVO₄ hybrids (Figure 5b,c), attesting to the critical role of the space-charge region in promoting the gas adsorption, which coincides well with the aforementioned TPD results.

Although the rationally designed space-charge region accelerates the adsorption of inert gas molecules, it is essential to explore the adsorption sequence of N₂ and CO₂ on the active sites to reveal the reaction mechanism. Compared with CO₂-TPD results, the peaks in the N₂-TPD spectrum emerge at a higher temperature and display the enhanced intensity, ensuring that N₂ gas preferentially adsorbs on the Bi-BiVO₄ hybrids than that of CO₂ molecule (Figure 4e,f).^[4] Notably, the bonded N₂ on the local electrophilic BiVO₄ region can be further activated by energetically preferred side-on configuration rather than end-on configuration (Figure 5d and Figure S11). It should be pointed out that the activation of the N₂ molecule needs to follow the previously reported “acceptance-donation” process. Herein, the empty e_g orbitals of V sites in VO₄ tetrahedron unit firstly accept the electrons from occupied σ orbitals of N₂ molecules, then the filled e_g orbitals of V sites donate their electrons to N₂ empty π^* orbitals, achieving the effective activation of N₂ molecule on the surface of the electrocatalyst (Figure 5e).

When comparing the Gibbs free energy (ΔG) of CO₂RR with and without the participation of N₂, one can conclude that the adsorbed N₂ molecule facilitates the reduction of CO₂ to CO (Figure 5f). Due to the *N=N* possesses the matched molecule orbitals with the released CO, the corresponding ΔG indicates that the formation of *NCON* intermediate is

exothermic (Figure 5g). Subsequently, the multi-step proton-coupled electron transfer process follows the two different pathways that is, distal pathway and alternating pathway. As shown in Figure 5g and Figure S12, for the case of distal mechanism, the (H⁺ + e⁻) continues to attack the distal N atom, while the (H⁺ + e⁻) alternatively reacts with N atoms on both sides when following the alternating mechanism. The potential-determining step during urea electrosynthesis is the generation of *NHCONH intermediate (*NCONH + H⁺ + e⁻ → *NHCONH, $\Delta G = 0.48$ eV) in the alternating pathway, whereas the reductive protonation of *NCONH into *NCONH₂ requires the highest ΔG value of 0.59 eV for the distal pathway. Thus, the hydrogenation of formed *NCON* will subsequently undergo the thermodynamically feasible alternating pathway until the release of the urea molecule.

The selectivity of the electrocatalytic urea production is closely associated with the formation of *NCON* species. At this stage, the possible N₂ reduction or the excessive release of CO would result in diverse product distribution and further reduce the selectivity of urea electrosynthesis. On the one hand, the competitive conversion of *N₂ into *NNH is inactive on the Bi-BiVO₄ hybrids, as shown in Figure S13. As seen, this process prefers to undergo at the pristine BiVO₄ model, which corroborates that the rationally designed space-charge region suppresses the NRR to some extent, let alone the generation of side product NH₃. On the other hand, the amount of CO should be well controlled. Once the active sites are strongly bonded with CO, which makes it difficult to couple with the adsorbed N₂ and thus retards the formation of *NCON* species. As exhibited in Figure S14, the correspond-

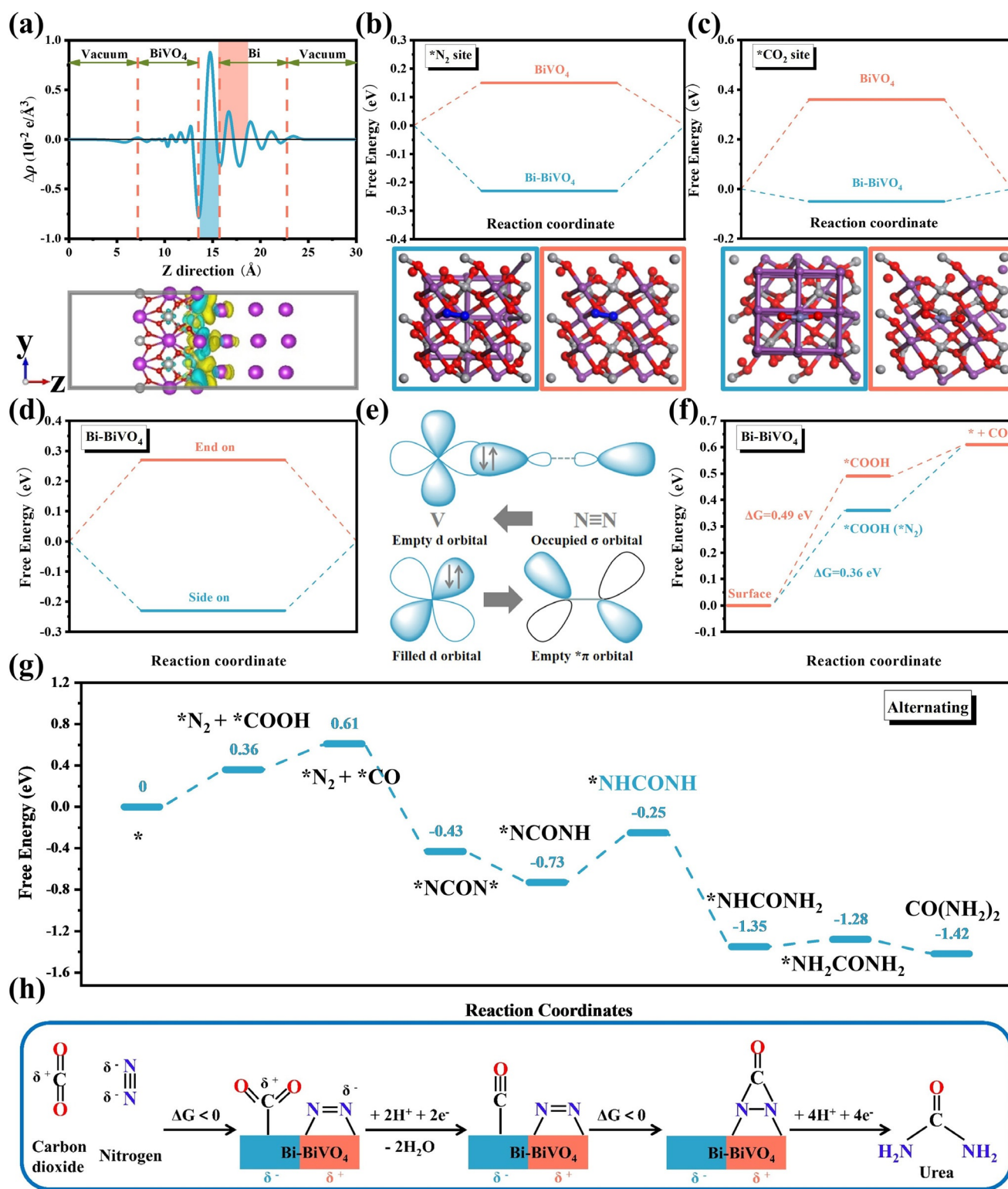


Figure 5. a) Top: Planar average charge density difference along the z-direction for the Bi-BiVO₄ heterojunction; bottom: charge density difference of the Bi-BiVO₄ heterojunction, yellow and cyan indicate electron accumulation and depletion, respectively, with isosurface values of 0.002 e/Å³. Free energy diagrams for b) N₂ and c) CO₂ adsorption on BiVO₄ and Bi-BiVO₄, the bottom figures are the corresponding calculation models; d) N₂ adsorbed on the Bi-BiVO₄ by different configurations; e) simplified schematic of N₂ bonding to V center; f) free energy diagrams for CO₂ reduction with and without N₂ adsorption on Bi-BiVO₄ hybrids; g) electrolytic urea production via the alternating mechanism; h) mechanism of the electrocatalytic urea synthesis based on synergistic effects of the Bi-BiVO₄ Mott-Schottky heterostructure.

ing electrochemical CO-stripping experiment results demonstrate that the CO-stripping peak of Bi-BiVO₄ hybrids

(0.258 V vs. RHE) displays the negatively shift compared with that of pristine BiVO₄ counterparts (0.345 V vs. RHE),

indicating the higher stability of Bi-BiVO₄ hybrids against CO poisoning, which is owing to the elimination of the part of strong adsorption sites by the presence of space-charge region.^[26] Conversely, the excessive release of CO is also not conducive to the urea electrosynthesis process. As shown in Figure 3e, beyond the applied potential of -0.4 V, the significantly reduced electrocatalytic urea production performance of the Bi-BiVO₄ hybrids can be ascribed to the occupation of the adsorption sites for N₂ and CO₂ by excessive release of CO.

By combining the aforementioned experimental results and computational simulations, the overall urea electrosynthesis process in Bi-BiVO₄ hybrids can be summarized as follows: (i) the spontaneous charge transfer at the hetero-interfaces promotes the formation of space-charge region, (ii) N₂/CO₂ molecules are firstly targeted adsorbed on the generated electrophilic/nucleophilic regions by electrostatic interaction, (iii) the adsorbed *N₂ can promote CO₂ reduction to form CO, and then the generated CO will further react with *N₂ to produce the desirable *NCON* intermediate via thermodynamically feasible electrochemical C-N coupling reaction, (iv) the subsequent protonation process preferentially undergoes the alternating mechanism until the formation of urea (Figure 5h).

Conclusion

In summary, the NaBH₄ reduction strategy was proposed to elaborately integrate metallic Bi and semiconductor BiVO₄ to form the Mott-Schottky heterojunction. The fabricated Bi-BiVO₄ hybrids achieve the maximum urea yield rate of 5.91 mmol h⁻¹ g⁻¹ and Faradaic efficiency of 12.55 % in 0.1 M KHCO₃ at -0.4 V vs. RHE. The space-charge region at the heterointerfaces induced by the self-driven charge transfer promotes the targeted adsorption and activation of inert N₂ and CO₂ molecules on generated local electrophilic and nucleophilic regions. Furthermore, the designed space-charge region also facilitates the electrocatalytic kinetics and enhances the full exposure of active sites, which contribute to the thermodynamically feasible coupling of the C-N bond and produce the desired *NCON* intermediate. Further exploration of the space-charge region may promote the fabricated electrocatalysts with the high urea electrosynthesis performance.

Acknowledgements

This work is supported by the National Key R&D Program of China (No. 2020YFA0710200) and the Chemistry and Chemical Engineering Guangdong Laboratory (No. 1922006). We also thank the financial project that Key Program for International S&T Cooperation Projects (No. 2018YFE0124600) funded by the Ministry of Science and Technology of China.

Conflict of interest

The authors declare no conflict of interest.

Keywords: C-N coupling · electrocatalysis · Mott-Schottky heterostructures · urea

- [1] a) M. D. Fryzuk, J. B. Love, S. J. Rettig, V. G. Young, *Science* **1997**, 275, 1445–1447; b) H.-P. Jia, E. A. Quadrelli, *Chem. Soc. Rev.* **2014**, 43, 547–564; c) T. Wu, H. Zhao, X. Zhu, Z. Xing, Q. Liu, T. Liu, S. Gao, S. Lu, G. Chen, A. M. Asiri, Y. Zhang, X. Sun, *Adv. Mater.* **2020**, 32, 2000299.
- [2] a) S. L. Foster, S. I. P. Bakovic, R. D. Duda, S. Maheshwari, R. D. Milton, S. D. Minter, M. J. Janik, J. N. Renner, L. F. Greenlee, *Nat. Catal.* **2018**, 1, 490–500; b) C. J. Pickett, J. Talarmin, *Nature* **1985**, 317, 652–653; c) T. Wang, Q. Liu, T. Li, S. Lu, G. Chen, X. Shi, A. M. Asiri, Y. Luo, D. Ma, X. Sun, *J. Mater. Chem. A* **2021**, 9, 884–888; d) R. Zhao, Q. Geng, L. Chang, P. Wei, Y. Luo, X. Shi, A. M. Asiri, S. Lu, Z. Wang, X. Sun, *Chem. Commun.* **2020**, 56, 9328–9331.
- [3] a) B. Obama, *Science* **2017**, 355, 126–129; b) A. D. Handoko, F. Wei, Jennndy, B. S. Yeo, Z. W. Seh, *Nat. Catal.* **2018**, 1, 922–934.
- [4] C. Chen, X. Zhu, X. Wen, Y. Zhou, L. Zhou, H. Li, L. Tao, Q. Li, S. Du, T. Liu, D. Yan, C. Xie, Y. Zou, Y. Wang, R. Chen, J. Huo, Y. Li, J. Cheng, H. Su, X. Zhao, W. Cheng, Q. Liu, H. Lin, J. Luo, J. Chen, M. Dong, K. Cheng, C. Li, S. Wang, *Nat. Chem.* **2020**, 12, 717–724.
- [5] a) K. A. Brown, D. F. Harris, M. B. Wilker, A. Rasmussen, N. Khadka, H. Hamby, S. Keable, G. Dukovic, J. W. Peters, L. C. Seefeldt, P. W. King, *Science* **2016**, 352, 448–450; b) X. Cheng, J. Wang, W. Xiong, T. Wang, T. Wu, S. Lu, G. Chen, S. Gao, X. Shi, Z. Jiang, X. Niu, X. Sun, *ChemNanoMat* **2020**, 6, 1315–1319; c) H. B. Yang, S.-F. Hung, S. Liu, K. Yuan, S. Miao, L. Zhang, X. Huang, H.-Y. Wang, W. Cai, R. Chen, J. Gao, X. Yang, W. Chen, Y. Huang, H. M. Chen, C. M. Li, T. Zhang, B. Liu, *Nat. Energy* **2018**, 3, 140–147.
- [6] a) D. M. Weekes, D. A. Salvatore, A. Reyes, A. Huang, C. P. Berlinguette, *Acc. Chem. Res.* **2018**, 51, 910–918; b) Z.-Q. Liang, T.-T. Zhuang, A. Seifitokaldani, J. Li, C.-W. Huang, C.-S. Tan, Y. Li, P. De Luna, C. T. Dinh, Y. Hu, Q. Xiao, P.-L. Hsieh, Y. Wang, F. Li, R. Quintero-Bermudez, Y. Zhou, P. Chen, Y. Pang, S.-C. Lo, L.-J. Chen, H. Tan, Z. Xu, S. Zhao, D. Sinton, E. H. Sargent, *Nat. Commun.* **2018**, 9, 3828; c) M. Yuan, Q. Li, J. Zhang, J. Wu, T. Zhao, Z. Liu, L. Zhou, H. He, B. Li, G. Zhang, *Adv. Funct. Mater.* **2020**, 30, 2004208.
- [7] Y. Feng, H. Yang, Y. Zhang, X. Huang, L. Li, T. Cheng, Q. Shao, *Nano Lett.* **2020**, 20, 8282–8289.
- [8] J. E. Kim, S. Choi, M. Balamurugan, J. H. Jang, K. T. Nam, *Trends Chem.* **2020**, 2, 1004–1019.
- [9] M. Aresta, A. Dibenedetto, A. Angelini, *Chem. Rev.* **2014**, 114, 1709–1742.
- [10] F. Barzagli, F. Mani, M. Peruzzini, *Green Chem.* **2011**, 13, 1267–1274.
- [11] a) Y. Ding, L. Huang, J. Zhang, A. Guan, Q. Wang, L. Qian, L. Zhang, G. Zheng, *J. Mater. Chem. A* **2020**, 8, 7229–7234; b) T. Wang, S. Li, B. He, X. Zhu, Y. Luo, Q. Liu, T. Li, S. Lu, C. Ye, A. Asiri, X. Sun, *Chin. J. Catal.* **2020**, 42, 1024–1029; c) T. Xu, B. Ma, J. Liang, L. Yue, Q. Liu, T. Li, H. Zhao, Y. Luo, S. Lu, X. Sun, *Acta Phys. Chim. Sin.* **2021**, 37, 2009043.
- [12] M. Yuan, H. Zhang, D. Gao, H. He, Y. Sun, P. Lu, S. Dipazir, Q. Li, L. Zhou, S. Li, Z. Liu, J. Yang, Y. Xie, H. Zhao, G. Zhang, *J. Mater. Chem. A* **2020**, 8, 2691–2700.
- [13] Z.-H. Xue, H. Su, Q.-Y. Yu, B. Zhang, H.-H. Wang, X.-H. Li, J.-S. Chen, *Adv. Energy Mater.* **2017**, 7, 1602355.

- [14] K. He, T. Tadesse Tsega, X. Liu, J. Zai, X.-H. Li, X. Liu, W. Li, N. Ali, X. Qian, *Angew. Chem. Int. Ed.* **2019**, *58*, 11903–11909; *Angew. Chem.* **2019**, *131*, 12029–12035.
- [15] a) M. Yuan, Y. Bai, J. Zhang, T. Zhao, S. Li, H. He, Z. Liu, Z. Wang, G. Zhang, *J. Mater. Chem. A* **2020**, *8*, 26066–26074; b) P. Lu, Y. Yang, J. Yao, M. Wang, S. Dipazir, M. Yuan, J. Zhang, X. Wang, Z. Xie, G. Zhang, *Appl. Catal. B* **2019**, *241*, 113–119.
- [16] Y. K. Kho, W. Y. Teoh, A. Iwase, L. Mädler, A. Kudo, R. Amal, *ACS Appl. Mater. Interfaces* **2011**, *3*, 1997–2004.
- [17] a) L. Sandhya Kumari, P. P. Rao, A. N. P. Radhakrishnan, V. James, S. Sameera, P. Koshy, *Sol. Energy Mater. Sol. Cells* **2013**, *112*, 134–143; b) F. D. Hardcastle, I. E. Wachs, *J. Phys. Chem.* **1991**, *95*, 5031–5041.
- [18] a) K.-H. Ye, X. Yu, Z. Qiu, Y. Zhu, X. Lu, Y. Zhang, *RSC Adv.* **2015**, *5*, 34152–34156; b) S. Xie, T. Zhai, Y. Zhu, W. Li, R. Qiu, Y. Tong, X. Lu, *Int. J. Hydrogen Energy* **2014**, *39*, 4820–4827.
- [19] a) T. Soltani, A. Tayyebi, B.-K. Lee, *Catal. Today* **2020**, *340*, 188–196; b) M. Balamurugan, G. Yun, K.-S. Ahn, S. H. Kang, *J. Phys. Chem. C* **2017**, *121*, 7625–7634.
- [20] a) D. Zhu, L. Zhang, R. E. Ruther, R. J. Hamers, *Nat. Mater.* **2013**, *12*, 836–841; b) M. Rahmatullah, T. R. C. Boyde, *Clin. Chim. Acta* **1980**, *107*, 3–9.
- [21] M. Alvarez-Guerra, J. Albo, E. Alvarez-Guerra, A. Irabien, *Energy Environ. Sci.* **2015**, *8*, 2574–2599.
- [22] M. Yuan, S. Dipazir, M. Wang, Y. Sun, D. Gao, Y. Bai, M. Zhang, P. Lu, H. He, X. Zhu, S. Li, Z. Liu, Z. Luo, G. Zhang, *J. Mater. Chem. A* **2019**, *7*, 3317–3326.
- [23] a) G. Zhu, X. Xie, X. Li, Y. Liu, X. Shen, K. Xu, S. Chen, *ACS Appl. Mater. Interfaces* **2018**, *10*, 19258–19270; b) M. Yuan, M. Wang, P. Lu, Y. Sun, S. Dipazir, J. Zhang, S. Li, G. Zhang, *J. Colloid Interface Sci.* **2019**, *533*, 503–512; c) C. Xi, G. Zhu, Y. Liu, X. Shen, W. Zhu, Z. Ji, L. Kong, *Colloids Surf. A* **2018**, *538*, 748–756.
- [24] D. Zang, Q. Li, G. Dai, M. Zeng, Y. Huang, Y. Wei, *Appl. Catal. B* **2021**, *281*, 119426.
- [25] Z. Geng, Y. Liu, X. Kong, P. Li, K. Li, Z. Liu, J. Du, M. Shu, R. Si, J. Zeng, *Adv. Mater.* **2018**, *30*, 1803498.
- [26] W. Zhang, Y. Yang, B. Huang, F. Lv, K. Wang, N. Li, M. Luo, Y. Chao, Y. Li, Y. Sun, Z. Xu, Y. Qin, W. Yang, J. Zhou, Y. Du, D. Su, S. Guo, *Adv. Mater.* **2019**, *31*, 1805833.

Manuscript received: January 27, 2021

Accepted manuscript online: February 25, 2021

Version of record online: April 8, 2021